Proposal for J-PARC 50 GeV Proton Synchrotron

Spectroscopic Study of Ξ-Hypernucleus, $^{12}_{\Xi}$Be, via the ^{12}C(K^-, K^+) Reaction

K. Aoki, M. Ieiri, T. Maruta, T. Nagae (Spokesperson), H. Noumi, Y. Sato,
S. Sawada, M. Sekimoto, H. Takahashi, T. Takahashi, A. Toyada
High Energy Accelerator Research Organization (KEK), Japan

Y. Fujii, O. Hashimoto, T. Ishikawa, H. Kanda, M. Kaneta, T. Koike, Y. Ma,
K. Maeda, K. Shirotori, S. N. Nakamura, H. Tamura, M. Ukai, H. Yamazaki
Tohoku University, Japan

P. K. Saha
Japan Atomic Energy Agency (JAEA), Japan

H. Fujioka, D. Nakajima, T. N. Takahashi
University of Tokyo, Japan

K. Nakazawa, T. Watanabe
Gifu University, Japan

K. Imai, K. Miwa, K. Tanida
Kyoto University, Japan

S. Ajimura, T. Kishimoto, A. Sakaguchi
Osaka University, Japan

M. Yosoi
Research Center for Nuclear Physics (RCNP), Osaka University, Japan

T. Fukuda
Osaka Electro-Communication University, Japan

P. Evtoukhovitch, V. Kalinnikov, W. Kallies, N. Kravchuk, A. Moiseenko,
D. Mzhavia, V. Samoilov, Z. Tsamalaidze, O. Zaimidoroga
Joint Institute for Nuclear Research (JINR), Russia

J. K. Ahn, B. H. Choi
Pusan National University, Korea

Y. Fu, C. Li, X. Li, C. Zhou, S. H. Zhou, L. H. Zhu
China Institute of Atomic Energy (CIAE), China

R. E. Chrien
Brookhaven National Laboratory (BNL), USA

B. Bassalleck
University of New Mexico, USA

J. Arvieux

IPN-O, Universite Paris-Sud, France

A. P. Krutenkova, V. V. Kulikov

Institute of Theoretical and Experimental Physics (ITEP), Russia

J. Reinhold

Florida International University, USA

B. Luigi, S. Marcello

Università di Torino, Italy

F. Diego

INFN, Sezione di Torino, Italy

M, Ombretta

INAF-IFSI, Sezione di Torino, Italy

L. Tang

Hampton University, USA

April, 28, 2006

Abstract

We propose to obtain the spectroscopic information of Ξ-hypernucleus, $^{12}_{\Xi}$Be, through the ^{12}C(K^-, K^+) reaction by using the high-intensity K^- beam at J-PARC. Ξ-hypernuclei, the existence of which is not well established so far, will be observed for the first time with enough statistics and a good energy resolution of $\sim$3 MeV. In order to perform such high-resolution spectroscopy, a new K^+ spectrometer will be constructed based on the existing SKS spectrometer. We request two weeks for the tuning of the new spectrometer system, and four weeks for the measurement of $^{12}_{\Xi}$Be with the K^- beam intensity of $1.6 \times 10^6 K^-$/spill.

The Ξ single-particle potential obtained from the observation of Ξ-hypernuclear states gives us not only the information on ΞN interaction but also insight into the high-density hadronic matter with strangeness. This experiment will be the first step to explore multi-strangeness hadronic systems which only J-PARC has an access to.
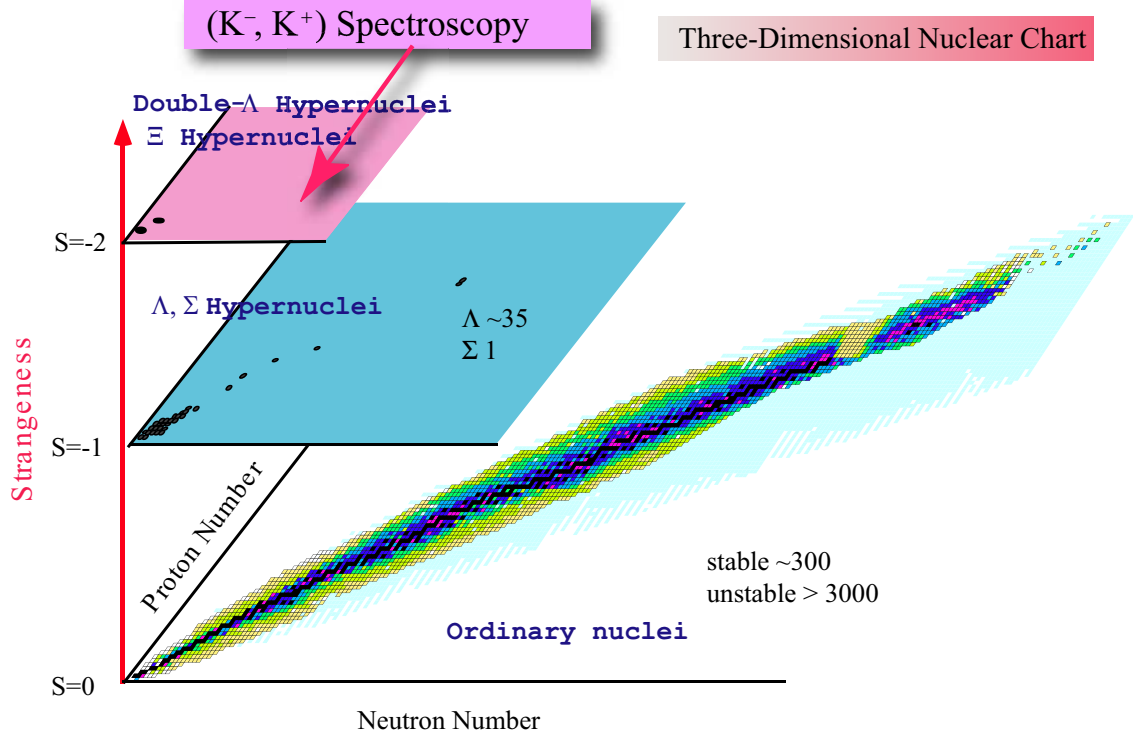
1

Figure 1: A three-dimensional nuclear chart with strangeness, S, as the third axis. On the $S = 0$ sheet, more than 3,000 nuclei including $\sim$300 stable ones are known, while about 35 Λ-hypernuclei and 1 Σ-hypernucleus are observed in the $S = -1$ systems. In the $S = -2$ systems, on the other hand, only a few double-Λ hypernuclei are known to exist at this moment.

1   Introduction

In 2002, we submitted Letter of Intent (LoI) for "New Generation Spectroscopy of Hadron Many-Body Systems with Strangeness $S = -2$ and -1"[1]. In the LoI, we proposed the construction of two separated kaon beam lines, namely, K1.8 and K1.1, to conduct three major research subjects; (1) spectroscopy of Ξ-hypernuclei, (2) study of double-Λ-hypernuclei by sequential pionic decays for $S = -2$ systems, and (3) γ-ray spectroscopy of Λ-hypernuclei for $S = -1$ systems. The LoI was classified as one of the two "Day-1" experiments by the Nuclear and Particle Physics Facility Committee (NPFC) in 2003. The NPFC recommended to construct the K1.8 beam line with high priority and encouraged us to consider the experimental plans in detail toward the full proposal.

This is the proposal to perform spectroscopy of Ξ-hypernuclei; one of the major researches mentioned in the LoI. We will observe $^{12}_{\Xi}$Be for the first time via the (K^-, K^+) reaction with a good energy resolution and enough statistics using high intensity K^-
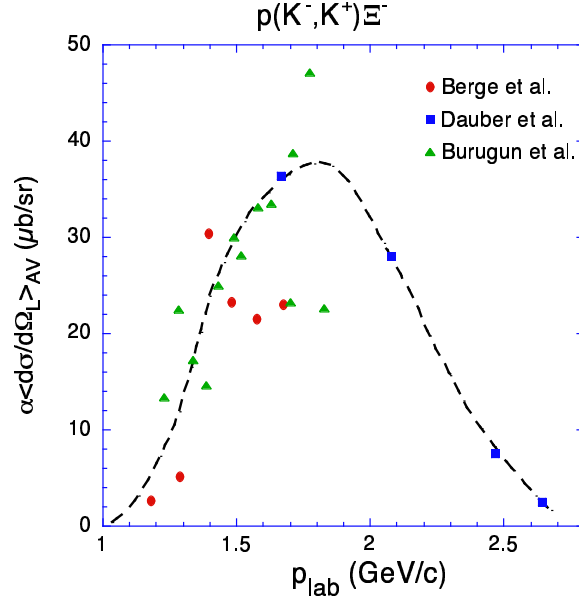
Figure 2: The incident momentum dependence of the forward angle laboratory cross section for $K^- p \rightarrow K^+ \Xi^-$ taken from ref.[2].

beams at K1.8 beam line and newly constructed high-resolution spectrometers. This will be the first but significant step toward future exploration to the multi-strangeness hadronic systems.

The high intensity K^- beam at $\sim$1.8 GeV/c available at J-PARC Hadron Facility is quite unique to open a new frontier of strangeness nuclear physics in the spectroscopic studies of strangeness $S = -2$ systems (Fig.1); here, the $S = -2$ systems include Ξ-hypernuclei, double-Λ-hypernuclei, and possibly H-hypernuclei. This is not only a step forward from $S = -1$ systems as a natural extension, but also a significant step to explore the multi-strangeness hadronic systems; in the course of the limit, strange hadronic matter ($S = -\infty$) in the core of a neutron star is our concern. It is also important to extract quantitative information on ΞN and $\Lambda\Lambda$ interactions from the spectroscopic data, considering the fact that there exists almost no data on these interactions at this moment. Hence, we can explore the SU(3) character of the strong forces of QCD.

1.1 Previous Studies on $S = -2$ Systems

The (K^-, K^+) reaction is one of the best tools to implant the $S = -2$ through the elementary process, $K^- p \rightarrow K^+ \Xi^-$, the cross section of which in the forward angle has a broad maximum around the momentum of 1.8 GeV/c as shown in Fig.2. This
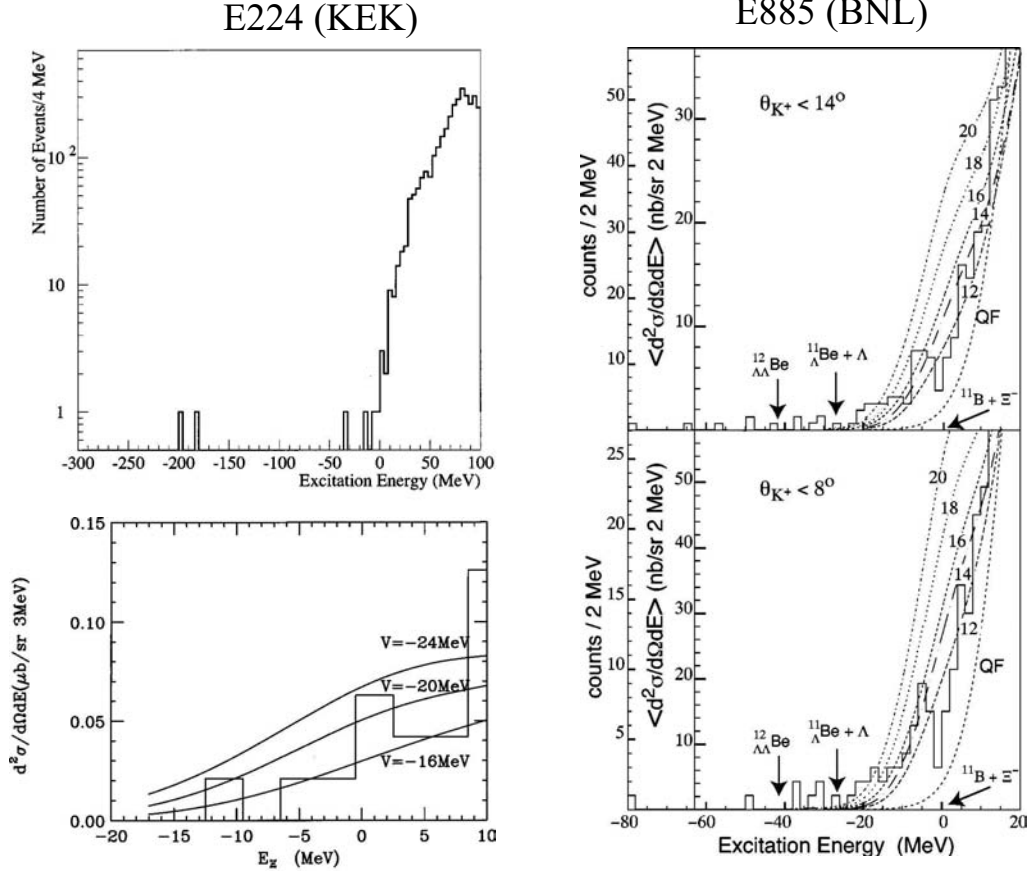
E224 (KEK)   E885 (BNL)

Figure 3: The missing mass spectra for ^{12}C(K^-, K^+) reaction obtained in KEK-E224 (left) and BNL-E884 (right) taken from ref.[9] and [10]. Curves in the figures are calculated spectra using various potential depths taking the experimental resolutions into account.

reaction has been used for studies of $S = -2$ systems so far.

As for the Ξ-hypernuclei, there exist some hints of emulsion events for the existence. However it is still not conclusive. Some upper limits on the Ξ-nucleus potential have been obtained from the production rate and spectrum shape in the bound region of Ξ-hypernucleus via ^{12}C(K^-, K^+) reaction[9, 10]. In these experiments, Ξ-hypernuclear states were not clearly observed because of the limited statistics and detector resolution (Fig.3). As shown in the figure, the potential depth, V_Ξ, is favored to be ~ -14 MeV for $A = 12$ when a Woods-Saxon type potential shape is assumed.

As for double-Λ-hypernuclei, several emulsion events were reported[3, 4, 5, 6, 7]. Among them, however, Nagara event recently found in a hybrid-emulsion experiment, KEK-PS E373, was able to be cleanly identify the $^6_{\Lambda\Lambda}$He. The mass of the $^6_{\Lambda\Lambda}$He and thus Λ-Λ interaction energy, $\Delta B_{\Lambda\Lambda}$, has been measured for the first time. It demonstrated

that Λ-Λ interaction is weakly attractive; weaker than that estimated before. The production of $^4_{\Lambda\Lambda}$H was also reported in a counter experiment by detection of pairs of pions in sequential mesonic weak decays[8]. However, $\Delta B_{\Lambda\Lambda}$ was not well determined due to poor statistics and the insufficient resolution.

A lot of searches for H-dibaryon have been carried out from the late 1980s to 1990s. No evidence has been observed so far. The observation of the weak decays from double-Λ hypernuclei limits the allowed mass range of the H very close to twice of mass of Λ. There are suggestions that H-particle may exist as a resonance and/or the "H"-type configuration might be mixed in the $S = -2$ systems.

1.2 Spectroscopy of Ξ-Hypernuclei and $S = -2$ Systems

The Ξ-hypernuclei will play an important role in the investigations of $S = -2$ systems as the entrance channel to the $S = -2$ world. In Fig.4, typical energy spectrum and decay threshold for Ξ- and double-Λ hypernuclear configurations are shown. Produced Ξ-hypernuclear states eventually decay into several forms of double-Λ systems through a strong conversion process, $\Xi^- p \to \Lambda\Lambda$. Moreover, Ξ-hypernuclei give valuable information on the $S = -2$ baryon-baryon interactions such as ΞN, and $\Xi N \to \Lambda\Lambda$. At this moment, we still even don't know whether the ΞN interaction is attractive or not, thus nor if Ξ-hypernuclei really exists or not. Although, the BNL E885 claims the evidence[10].

While single-Λ and double-Λ hypernuclear ground states decay via weak interaction and therefore they are long-lived, Ξ-hypernuclei decay via the strong interaction through a conversion process $\Xi^- p \to \Lambda\Lambda$ (Q=28.3 MeV). This situation is very similar to Σ-hypernuclei in which the strong conversion process $\Sigma N \to \Lambda N$ ($Q \sim$75 MeV) also exists and broadens the width of the states. However, $\Xi^- p \to \Lambda\Lambda$ conversion occurs in the $^1S_0(T$=0$)$ state, a weight of which is only 1/16 even in the nuclear matter. Although it depends on the interaction models, the width for finite nuclei may be reduced to $\leq$1 MeV due to the reduction of the phase space and the reduction of an overlap of the wave functions. The calculated widths in several interaction models are listed in Table 1 for the nuclear matter and Table 2 for finite nuclei.

Therefore, it is expected that the spectroscopy of the Ξ-hypernuclei is promising. Here we use the (K^-, K^+) reaction in which we can use the same method as in the (π^+, K^+) reaction succeeded for the Λ-hypernuclear spectroscopy. The (K^-, K^+) reaction has the following characteristics in comparison with the (π^+, K^+) reaction.

1. A Ξ^- is produced with a large recoil momentum similar to a Λ for the (π^+, K^+) reaction; $p_\Xi \sim$500 MeV/c and $p_\Lambda \sim$350 MeV/c. Due to the large momentum transfer of the reaction, spin-stretched states can be selectively populated as in the case of Λ-hypernuclei by the (π^+, K^+) reaction. This selectivity helps us to observe well-separated peak structures even for heavy targets among many possible excitations.
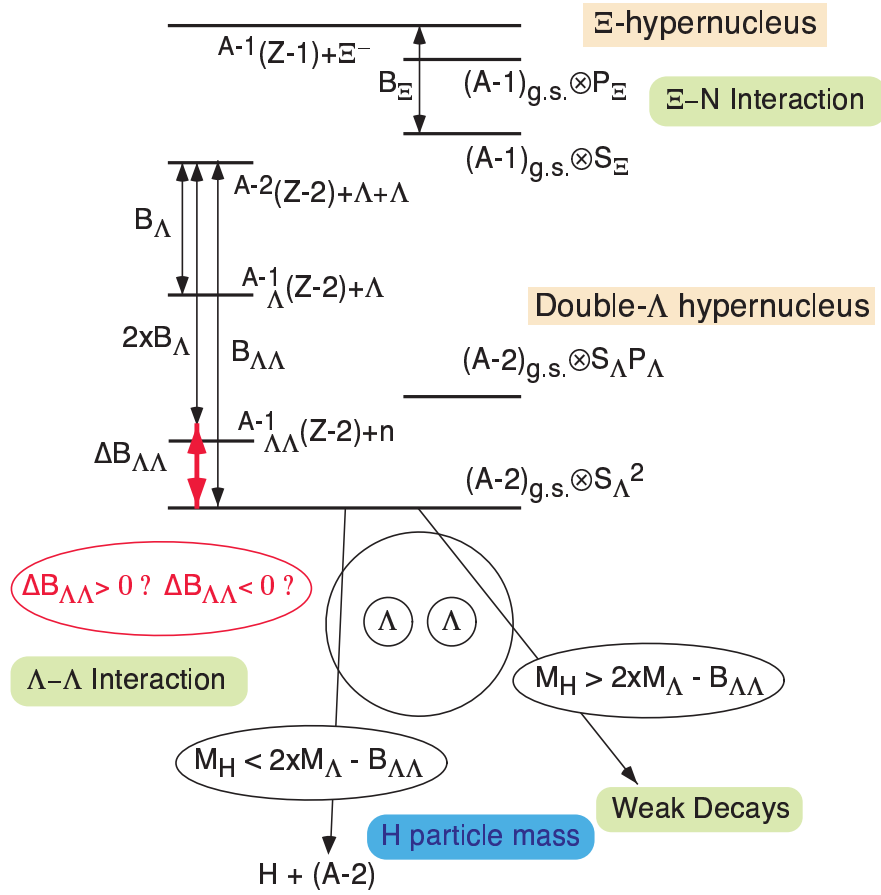
Figure 4: Typical energy spectrum and decay threshold for $S = -2$ system; Ξ- and double-Λ hypernuclear configurations.

2. The large momentum transfer of the reaction, however, means small nuclear form factors. The transition form factors (c.f. overlap of the wave functions) are smaller than those for the (π^+, K^+) reaction. Therefore smaller production cross section is expected.

3. The (K^-, K^+) reaction converts a proton to a Ξ^- with double charge exchange, while the (π^+, K^+) reaction converts a neutron to a hyperon. Therefore the produced hypernuclei are neutron-rich in general.

4. In other word, the isospin transfer of the reaction is 1. Therefore only the states of $\Delta T = 1$ transition can be excited.

5. There could be a possibility to have some strengths for unnatural-parity (spin-
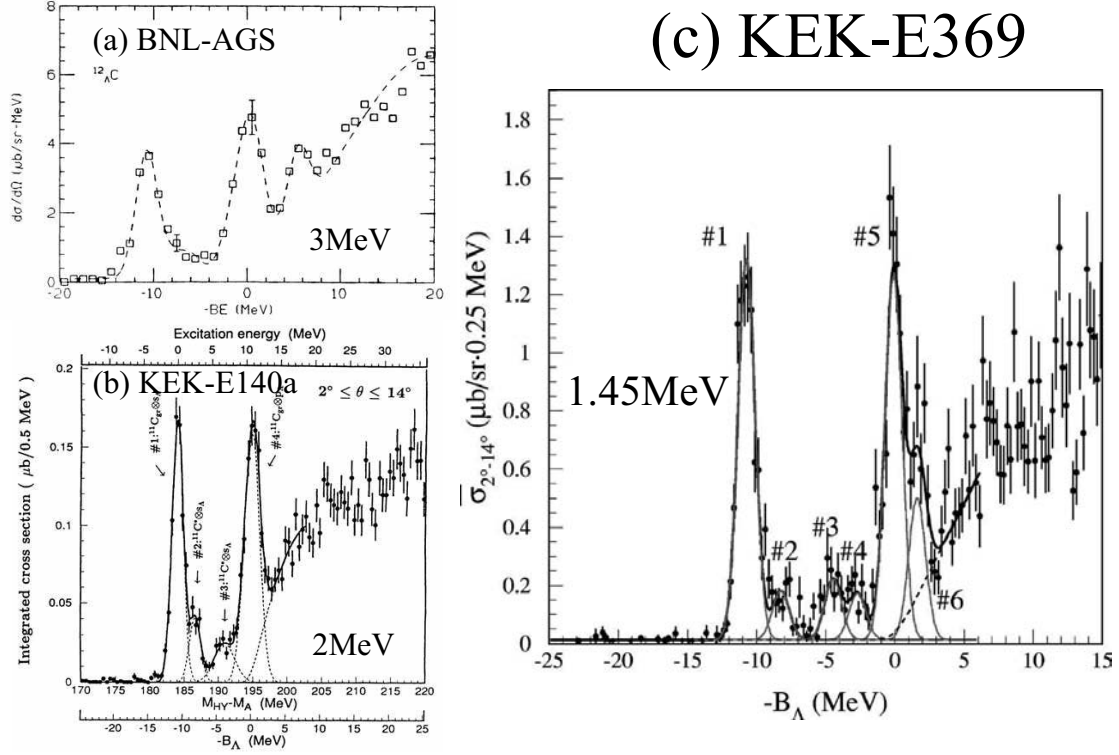
Figure 5: $^{12}_{\Lambda}$C spectra measured in the ^{12}C(π^+, K^+) reaction at BNL (a)[14], KEK E140a (b)[15], and KEK E369 (c)[16]. Missing mass resolutions are 3, 2, and 1.45 MeV (FWHM), respectively.

flip) transitions, while no reliable prediction exists. The data on the elementary production [11, 12] are too uncertain to conclude whether spin-flip amplitude is sizable[13].

6. The cross section of the elementary $p(K^-, K^+)\Xi^-$ process is considerably smaller than that of the $n(\pi^+, K^+)\Lambda$ reaction; 35 μb/sr for the (K^-, K^+), while $\sim$500 μb/sr for the (π^+, K^+).

In spite of several demerits such as a small cross section, the (K^-, K^+) reaction is the best tool for the reaction spectroscopy of Ξ-hypernuclei. The previous studies were not able to clearly conclude the existence of the Ξ-hypernuclear states. This is because that their detector resolution was not so good to identify the states and the statistics was not enough to detect the states with such small cross sections.

The good resolution is crucial for the spectroscopy as demonstrated in Fig.5 for Λ-hypernuclear spectroscopy. The figure shows $^{12}_{\Lambda}$C spectra obtained in the ^{12}C(π^+, K^+) reaction at BNL[14], KEK E140a[15], and KEK E369[16], the resolutions of which were 3, 2, and 1.45 MeV (FWHM), respectively. Thanks to the best energy resolution of

7

Table 1: Ξ potentials U_Ξ and partial wave contributions in nuclear matter at normal density, calculated with NHC-D, Ehime and ESC04d*. Conversion widths in nuclear matter, Γ_Ξ, is also listed. Unit is MeV.

Model	T	$^1S_0$	$^3S_1$	$^1P_1$	$^3P_0$	$^3P_1$	$^3P_2$	U_Ξ	Γ_Ξ
NHC-D	0	-2.6	0.1	-2.1	-0.2	-0.7	-1.9		
	1	-3.2	-2.3	-3.0	-0.0	-3.1	-6.3	-25.2	0.9
Ehime	0	-0.9	-0.5	-1.0	0.3	-2.4	-0.7		
	1	-1.3	-8.6	-0.8	-0.4	-1.7	-4.2	-22.3	0.5
ESC04d*	0	6.3	-18.4	1.2	1.5	-1.3	-1.9		
	1	7.2	-1.7	-0.8	-0.5	-1.2	-2.8	-12.1	12.7

1.45 MeV, several core-excited states were clearly resolved in KEK E369.

Therefore it is important to perform the reaction spectroscopy again by using the high-intensity K^- beams at J-PARC and the spectrometers with a much improved energy resolution. Convincing evidence for Ξ single-particle states would yield information on Ξ single-particle potential and the effective ΞN interaction. Several topics are described bellow.

1.2.1 ΞN Interaction Model and Ξ-Hypernuclei

Since little is known for $S = -2$ baryon-baryon systems, especially ΞN system, there is no established interaction model in $S = -2$ channels. This is mainly due to the lack of experimental data such as ΞN elastic and inelastic scattering. As a consequence, the derived one-body Ξ potentials, U_Ξ, are remarkably different among the available interaction models. In some cases, they are even repulsive. Therefore the experimental determination of U_Ξ is decisively important in order to obtain a reasonable interaction model.

Here, we briefly show the calculation results[17] in three different interaction models;

- Nijmegen Hard-Core model D (NHC-D)[18]

- Ehime model[19]

- Extended Soft-Core model 04d* (ESC04d*)[20]

These models give attractive (negative) value of U_Ξ. The details of the interaction models are described in Appendix.A.

Table 1 shows the calculated values of Ξ potential (U_Ξ), conversion width (Γ_Ξ) and partial wave contribution in nuclear matter obtained in the G-matrix calculations with three interaction models. In Table 2, the energies and widths for the Ξ^- bound states produced via the (K^-, K^+) reaction on ^{12}C, ^{27}Al, ^{40}Ca, ^{89}Y are listed for four different

Table 2: Energies, widths and mean radii, $\overline{r} = \sqrt{<r^2>}$, predicted by NHC-D, Ehime and ESC04d*. The Ξ^--nucleus potentials are obtained by folding the ΞN G-matrix interactions. The results for the Woods-Saxon potential with $V_\Xi^0 = -14$ MeV are also listed.

	NHC-D			Ehime			ESC04d*			W.S.
Target	E	Γ	$\overline{r}$	E	Γ	$\overline{r}$	E	Γ	$\overline{r}$	E
	[MeV]	[MeV]	[fm]	[MeV]	[MeV]	[fm]	[MeV]	[MeV]	[fm]	[MeV]
^{12}C [$^{12}_\Xi$Be]										
s	-4.4	0.5	3.2	-4.5	0.3	3.1	-4.6	4.6	3.3	
w/o Coulomb	-1.9	0.5	3.7	-1.9	0.2	3.7	-2.1	3.9	3.7	-2.2
^{27}Al [$^{27}_\Xi$Na]										
s	-14.9	0.7	2.0	-13.4	0.2	2.3	-10.1	5.7	3.0	
w/o Coulomb	-8.4	0.7	2.2	-7.3	0.2	2.6	-4.7	4.7	3.4	-5.1
p	-7.1	0.4	3.4	-5.9	0.2	3.6	-5.2	2.8	4.1	
w/o Coulomb	-2.0	0.3	4.0	-1.1	0.1	4.5	-0.8	1.9	5.1	
^{40}Ca [$^{40}_\Xi$Ar]										
s	-19.7	0.6	2.2	-18.7	0.2	2.4	-14.1	5.9	3.0	
w/o Coulomb	-10.8	0.6	2.4	-9.9	0.2	2.6	-6.2	4.9	3.4	-6.5
p	-13.7	0.5	3.0	-11.5	0.2	3.3	-9.3	3.3	3.9	
w/o Coulomb	-5.7	0.4	3.3	-3.9	0.2	3.7	-2.4	2.5	4.5	-1.2
^{89}Y [$^{89}_\Xi$Rb]										
s	-31.4	0.6	2.3	-29.8	0.2	2.5	-22.4	6.5	3.0	
w/o Coulomb	-16.4	0.6	2.5	-15.0	0.2	2.8	-8.5	5.2	3.7	-9.0
p	-26.2	0.5	3.0	-23.6	0.2	3.3	-17.8	3.9	4.0	
w/o Coulomb	-12.0	0.4	3.2	-9.8	0.2	3.6	-5.3	2.8	4.6	-4.6
d	-20.6	0.4	3.5	-17.3	0.2	3.9	-13.3	2.4	4.7	
w/o Coulomb	-7.3	0.3	3.9	-4.6	0.1	4.4	-2.0	1.7	5.5	-0.2
f	-14.8	0.3	4.1	-11.0	0.1	4.6	-8.7	1.6	5.4	

potentials; three Ξ-nucleus potentials obtained from the ΞN G-matrix interaction and a simple Woods-Saxon type potential with the depth of -14 MeV. It should be noted that NHC-D and Ehime models predict deep U_Ξ and strong mass-number (A) dependence for Ξ energies. This is owing to the strong odd-state attractions which come from the lack of space-exchange terms in one-boson-exchange potential picture. On the other hand, ESC04d* model predicts the energies very close to those with the Woods-Saxon potential, when the Coulomb interactions are switched off. Therefore, the experimental data on not only the Ξ-binding energies but also the their A-dependence have valuable information to probe the ΞN interaction. It should be also noted that the conversion widths for ESC04d* and NHC-D/Ehime are very different from each other.

For s- and light p-shell systems, NHC-D and Ehime give rise to almost no Ξ bound state because of their weak even-state attractions, when the Coulomb interactions are

switched off. In the case of ESC04d*, however, interesting Ξ bound states such as $^4_\Xi$H(0^+) are produced owing to the strong attraction in the $^3S_1(T = 0)$ state. Unfortunately, most of them cannot be produced through the (K^-, K^+) reaction. One interesting possibility is to use a proton-rich target such as ^{3}He.

1.2.2 Ξ Potential and Hadronic Matters

Knowledge of the depth of the Ξ-nucleus potential is also important for estimating the existence of strange hadronic matter with Ξ. For a long time, it was believed that Σ^- hyperons would appear in neutron stars earlier (i.e. at lower density) than even lighter Λ hyperons due to their negative charge. However, recent data[21], strongly suggest that the interaction of the Σ^- with neutron-rich nuclear systems is strongly repulsive, which means Σ^- hyperons can no longer appear in neutron stars. It was argued that the disappearance of Σ^- does not necessarily leads to crucial changes of neutron star features if they were substituted effectively by Ξ^- hyperons. Furthermore, it is also argued quite recently that even K^- mesons may appear in neutron stars after the discovery of deeply-bound kaonic nuclear systems[22, 23, 24]. However better understanding of ΞN interaction is necessary for a definite conclusion. With respect to the structure of the neutron star, it becomes much more important to investigate the Ξ dynamics than it was considered previously because the Σ-nucleus repulsion has been established.

1.2.3 Mixing of Other $S = -2$ States

It has been discussed the possibilities of the mixing between Λ- and Σ-hypernuclear states in $S = -1$ system through the ΣN-ΛN couping. For example, the admixture of Σ states is estimated approximately 1% at $A = 4$ hypernuclei[25]. This coupling interaction also produces 3-body force via $(N$-$\Lambda)$-$N \rightarrow N$-Σ-$N \rightarrow N$-$(\Lambda$-$N)$. The mixing and the 3-body force are important to reproduce the energy levels for few body Λ-hypernuclear systems. In the case of $S = -2$ systems, on the other hand, the mass difference between ΞN and $\Lambda\Lambda$ is much smaller ($\sim$28 MeV) than the one between ΣN and ΛN ($\sim$75 MeV) for $S = -1$ systems. Therefore the state-mixing and the mixing process are expected to play more important roles in $S = -2$ systems than in $S = -1$ systems.

The existence of $^4_{\Lambda\Lambda}$H is brought in question by many authors[26, 27]. The $\Lambda\Lambda$ interaction deduced from $^6_{\Lambda\Lambda}$He is so weak that $pn\Lambda\Lambda$ system is not bound in simple calculations. However, it is argued recently that this contradiction can be resolved if one takes the ΞN-$\Lambda\Lambda$ couping into account when the ΞN interaction is attractive[28]. Therefore the nature of the ΞN interaction affects the existence of light double Λ hypernuclei and thus the $\Lambda\Lambda$ interaction deduced from them.

1.2.4 Observation of Double-Λ Hypernuclei

Through the (K^-, K^+) reaction, double-Λ hypernuclei could be produced directly through a two-step process, $K^- p \rightarrow \Lambda(\pi^0, \rho^0, \omega)$, $(\pi^0, \rho^0, \omega)p \rightarrow K^+\Lambda$ or $K^- p \rightarrow K^+\Xi^-$, $\Xi^- p \rightarrow \Lambda\Lambda$. Since these double-$\Lambda$ hypernuclear states are kinematically separated from the Ξ-hypernuclear states, we can easily identify these states with good energy resolution of $\sim$3 MeV. However, a theoretical estimation for $^{16}O(K^-, K^+)^{16}_{\Lambda\Lambda}C$[29] suggests a very small cross section for the ground state but a few nb/sr for the excited states at 1.1 GeV/c. If there were large mixing between Ξ hypernuclear states and the excited levels of double-Λ hypernuclei, some enhancements would be expected for the excitation. This method has a unique advantage to allow us direct access to the excited states of double-Λ hypernuclei.

There are a lot of interesting and important physics in the study of the Ξ-hypernucleus of new $S = -2$ world. It is emphasized here that the J-PARC is the only facility in the world which can explore the $S = -2$ world.

2 Purpose of the Proposed Experiment

Main physics goal of the experiment proposed here is to obtain the conclusive results on the existence of Ξ-hypernuclei by observing bound states of Ξ hypernuclei via the (K^-, K^+) reaction with the best energy resolution of a few MeV so far achieved and in large statistics. For this purpose, we will construct two high-resolution spectrometers for K^- beam and scattered K^+'s.

We will measure the $^{12}C(K^-, K^+)$ reaction as a first step of a series of measurements on various targets. This is because the previous BNL measurement with the same reaction claimed a substantial number of events in the bound region of $^{12}_{\Xi}$Be, and the production cross section was estimated already although the statistical error was large. Thus, a rather reliable design of the experiment is possible for this reaction. An unambiguous experimental observation of Ξ-hypernuclear bound states is very significant progress even in a single target.

Further, in the previous measurement, the potential depth of $\sim$14 MeV was extracted from the shape analysis near the Ξ binding threshold with a help of theoretical calculations. It suggests that we could definitely observe a bound state peak distinguished from the quasi-free continuum as shown in Fig.6. This figure shows the calculated spectra for the $^{12}C(K^-, K^+)^{12}_{\Xi}$Be reaction for Woods-Saxon Ξ^- potential with the depths of -14 MeV and -20 MeV without smearing the experimental resolution [10]. The figure demonstrates the importance of the good resolution of the measurements when one compares it with the right-top of Fig.3. A peak position will give us more direct information of the depth of Ξ-nucleus potential than the previous shape analysis.

The width of the bound state peak also has information on the imaginary part of the Ξ-nucleus potential, or the ΞN inelastic channel. Thus, even no observation of
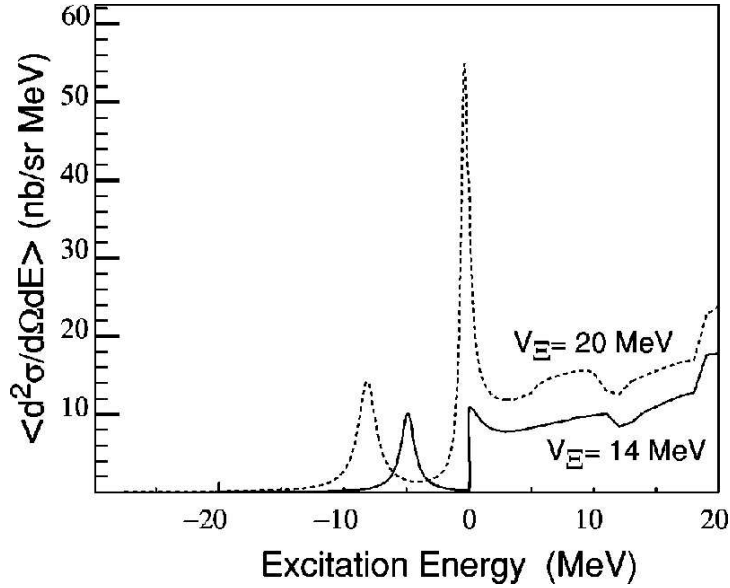
Figure 6: The calculated spectrum for ^{12}C$(K^-, K^+)^{12}_\Xi$Be reaction for Ξ potential depths of -14 MeV (solid) and -20 MeV (dotted) taken from ref.[10]. The cross section has been averaged over the kaon angular range from $0°$ to $14°$.

clear peaks is also informative because it may be due to a large spreading width. On that account, a well experimental control of the energy resolution in the measurement is very important. Fortunately, we can use the elementary process of $K^- p \to K^+ \Xi^-$ for this calibration with a CH$_2$ target.

Anyway, nobody has ever succeeded to observe any peaks for Ξ-hypernuclei or double-Λ hypernuclei in the (K^-, K^+) spectroscopy. Therefore, at this moment, we think it is important to establish the methodology of the (K^-, K^+) spectroscopy like we did it for the (π^+, K^+) spectroscopy. Here the methodology means not only the hardware devices such as a beam line spectrometer, a high-resolution K^+ spectrometer, etc. but also know-hows to operate the new devices keeping good performances, to understand the production rate and backgrounds, and to even establish the analysis method. Once the methodology is well established, it is relatively easy to plan further measurements on other targets or other objects such as double-Λ hypernuclei with some modifications and/or upgrade of the detectors. In this regard, we think the ^{12}C(K^-, K^+) reaction is the best choice to start with.

Table 3: Design parameters of K1.8 beam line

		Phase-II (50GeV-15μA)	Phase-I (30GeV-9μA)
Max. Mom.	[GeV/c]		2.0
Length	[m]		45.853
Acceptance	[msr·%]		1.4
Electro-static Separator		750 kV/10 cm, 6 m × 2	
K^- Intensity	[/spill]		
	1.8 GeV/c	6.6×10^6	1.4×10^6
	1.1 GeV/c	3.8×10^5	8.0×10^4
K^-/π^- @ FF	@ 1.8 GeV/c	8	6.9
X / Y(rms) size @ FF	[mm]	19.8 / 3.2	
Singles-rate @ MS2	@ 1.8 GeV/c	$>3.3 \times 10^7$	$>8 \times 10^6$

3 Experimental Methods and Apparatus

Ξ hypernuclei are produced via the (K^-, K^+) reaction. As described in ref.[2], the forward-angle laboratory (differential) cross section of the elementary process, $K^- p \to K^+ \Xi^-$, peaks at around the incident momentum of 1.8 GeV/c. In the case of nuclear targets, the momentum dependence is somewhat smeared out by Fermi motion. However, the optimal beam momentum is also around 1.8 GeV/c. In this case, the outgoing K^+ momenta range from 1.3 to 1.4 GeV/c. Produced hypernuclear states are measured as a missing mass of the reaction. Therefore, we need spectrometers with a good resolution both for the incident beam and the outgoing particles.

3.1 K1.8 Beam Line and Beam Analyzer

Design work of the K1.8 beam line was already finished by the J-PARC hadron beam line construction group after NPFC meeting held in 2004. Figure 7 shows a beam line layout together with the K^+ spectrometer in the K1.8 experimental area. In Table 3, design parameters are listed. Figure 8 shows beam envelope of the K1.8 beam line calculated by *TRANSPORT*. The beam line has two characteristic features; (1) high-intensity and high-purity K^- beams are obtained. (2) a high resolution beam analyzer is located at the end of the beam line. These features are required and optimized to perform the spectroscopic studies on Ξ-hypernuclei.

The beam line has two stages of electro-static separators (ES1 and ES2) with two mass slits (MS1 and MS2) in order to separate kaons from pions and other particles at the level of K^-/π^- ratio greater than 5. Optimization study of the shape of the mass slits is still in progress in order to further improve the K^-/π^- ratio and decrease the unwanted particle rate at the upstream of the beam analyzer.
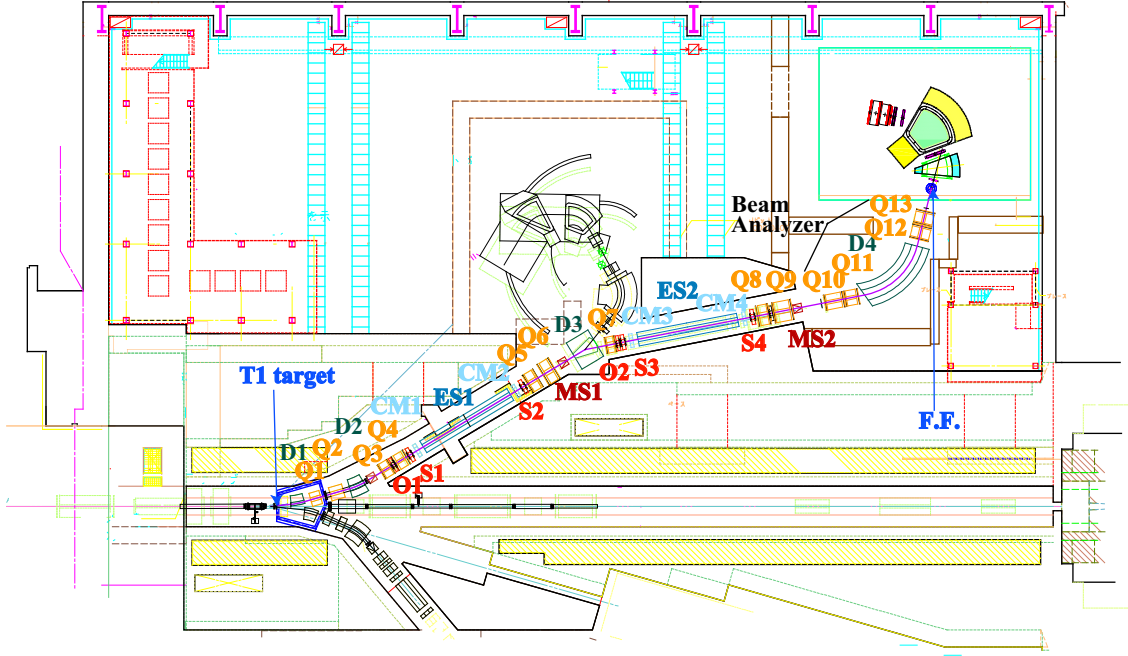
Figure 7: The layout of K1.8 beam line and K1.8 area.

The beam analyzer located after MS2 comprises $QQDQQ$ magnets and four sets of tracking detectors. The $QQDQQ$ optics is tuned to point-to-point focus condition and $< X|\theta >= 0$ in order to minimize the multiple scattering effect on the resolution. The expected momentum resolution $\Delta p/p$ is 1.4×10^{-4} in rms when a position resolution of 200 μm is realized in the tracking detectors placed before and after the $QQDQQ$ system.

The tracking detectors are one of the most important detectors in the beam line. They should be as thin as possible to keep good energy or momentum resolution of the beam analyzer. They should also work with good enough resolutions and good efficiencies under high-rate environment. When we use flat top of 0.7 seconds operation at the Phase-I full intensity (30GeV-9μA), the charged particle rate at downstream of the $QQDQQ$ magnet is expected to be $1.4\times10^6 \times(7.9/6.9) / 0.6 = 2.67 \times 10^6$/sec.. Higher rate of one order of magnitude is expected at the upstream of the $QQDQQ$, due to the kaons not decayed yet and other background particles scattered at MS2 etc. A wire chamber is one of such detectors with thin materials and high-rate capability. At KEK-PS K6 beam line, we could operate drift chambers with the anode-spacing of 5 mm under $3 - 4 \times10^6$ pions/spill on the target with the flat-top length of 2.0 seconds. The particle rate at the upstream of the beam spectrometer was estimated
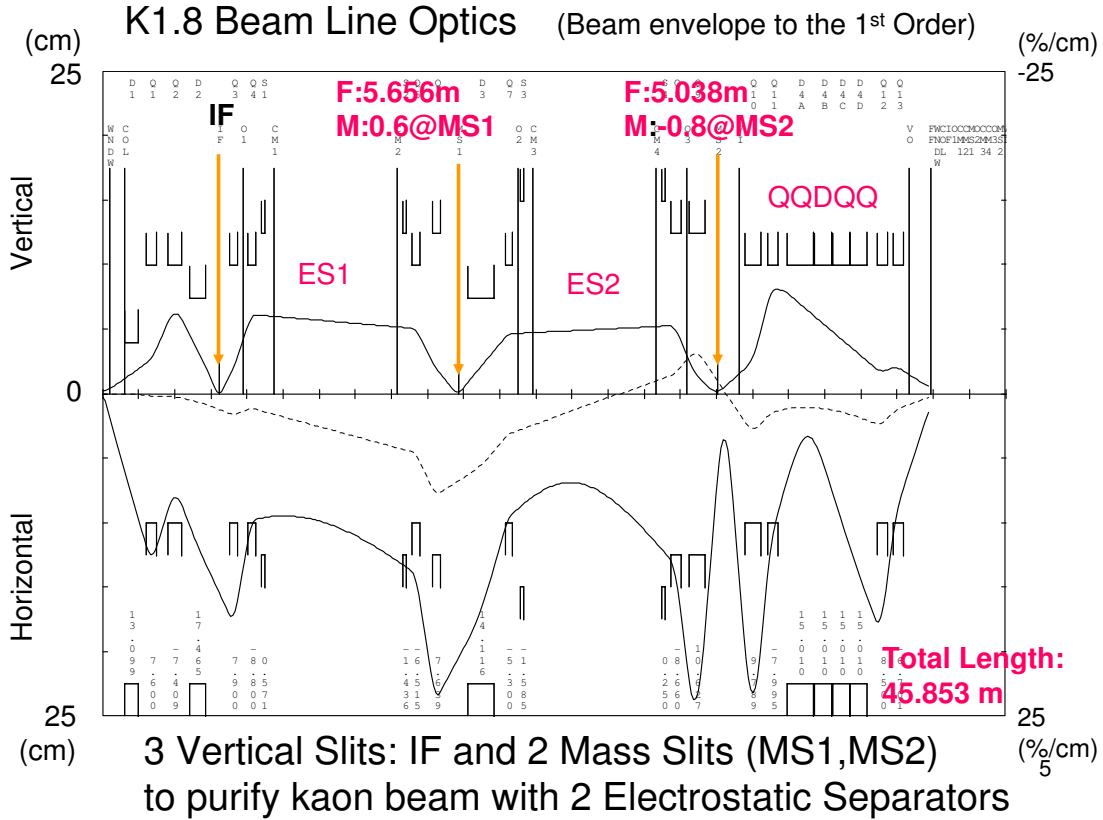
14

Figure 8: Beam envelope of the K1.8 beam line calculated by *TRANSPORT*.

to be twice as high as that at the downstream. Thus, these chambers should be able to be operated under the rates of 4×10^6 / $2 \times 2 = 4 \times 10^6$ /second. Taking account of the beam size, we will use MWPCs with 1 mm anode pitch and drift chambers with anode pitch of 3 mm at the upstream and downstream parts of the $QQDQQ$ magnets, respectively.

Segmented plastic scintillator hodoscopes will be located at the upstream and downstream of the beam analyzer for trigger and offline particle identification. Aerogel Cerenkov counter located just upstream of the target (BAC) will be also used in the trigger level. Time of flight measurement between two beam hodoscopes whose distance is ∼8 m can separate kaons from pions at 1.8 GeV/c in offline analysis.
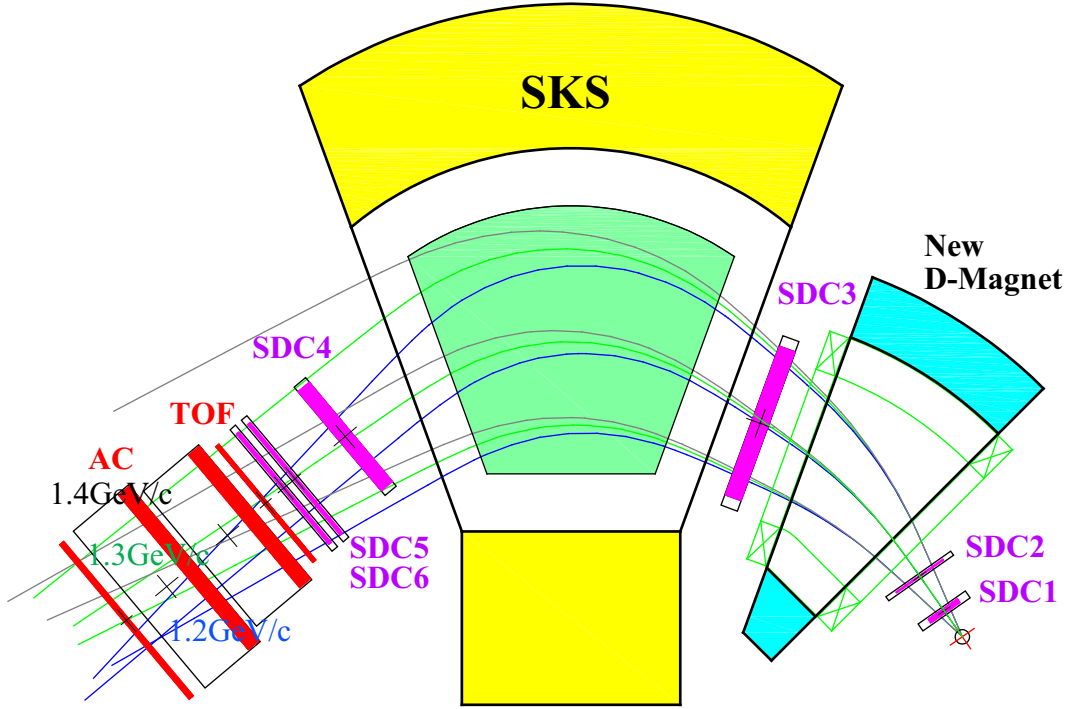
Figure 9: SksPlus Spectrometer in consideration.

3.2 Spectrometer for Scattered Particles

For the K^+ spectrometer, we will use the existing SKS spectrometer with some modifications. The K^+ momentum corresponding to the production of Ξ-hypernuclei is around 1.3 GeV/c. The SKS maximum magnetic field of $\sim$2.7 T does not allow us to put the central ray at 1.3 GeV/c. Therefore, the central ray is shifted outer side and a dipole magnet with $\sim$1.5 T will be added at the entrance of the SKS magnet as shown in Fig.9. Although a detailed design is still in progress, a simulation shows that the spectrometer, (called as SksPlus), has a solid angle of $\sim$30 msr with the angular range up to 10° , and momentum resolution $\Delta p/p = 0.17\%$ (FWHM) when the position resolution of 300 μm in rms is achieved. (Fig.10)

We will use 6 sets of drift chambers (SDC1–6) as tracking detectors of the SksPlus spectrometer. The SDC1 and SDC2 located after the target should be high-rate chambers, since the beam particles will directly pass through. These chambers are similar to the beam line chambers except for the size. Other chambers do not require high-rate capability, because the beam does not pass through these detectors thanks to the double-charge-exchange reaction. The SDC3 will be installed between the newly installed dipole magnet and the SKS magnet in order to tune up the spectrometer optics
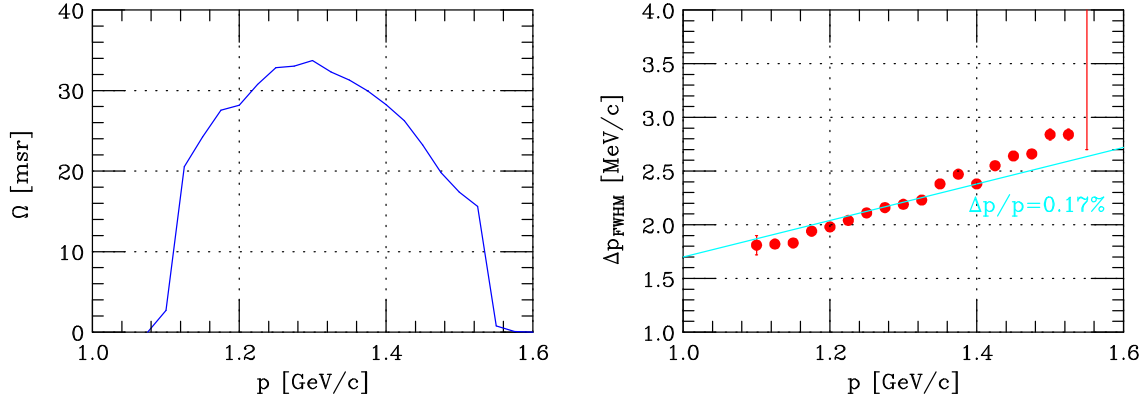
16

Figure 10: Momentum acceptance (left) and resolution (right) of the SksPlus spectrometer from simulation.

etc. Once we understand the optics and establish the analysis method, this detector may be removed in order to avoid multiple scattering.

For trigger and particle identification, the following detectors will be used; TOF wall, Aerogel Cerenkov counters (AC), Lucite Cerenkov counter (LC), and possibly water Cerenkov counter. These detectors as well as SDC4–6 are reused ones in the existing SKS detectors.

3.3 Missing Mass Resolution

The energy resolution is a key point in the experimental point of view for the spectroscopy. The resolution should be better than the spacing of the hypernuclear levels and comparable to or better than the widths of the states. Here the energy resolution is estimated.

Missing mass, M, is expressed as,

$$
\begin{aligned}
M^2 &= (E_B + m_T - E_S)^2 - (\vec{p}_B - \vec{p}_S)^2 \\
&= m_B^2 + m_S^2 + m_T^2 + 2\left(m_T E_B - m_T E_S - E_B E_S + p_B p_S \cos\theta\right),
\end{aligned} \tag{1}
$$

where θ is scattering angle, m, E, $\vec{p}$ and p are mass, energy, three-momentum and magnitude of the momentum, respectively. Suffixes B, S and T mean beam and scattered particles, and target, respectively. By differentiating above equation, missing mass resolution, ΔM is expressed as follows,

$$
\Delta M^2 = \left(\frac{\partial M}{\partial p_B}\right)^2 \Delta p_B^2 + \left(\frac{\partial M}{\partial p_S}\right)^2 \Delta p_S^2 + \left(\frac{\partial M}{\partial \theta}\right)^2 \Delta\theta^2 + \Delta E_{\text{strag.}}^2, \tag{2}
$$

$$
\frac{\partial M}{\partial p_B} = \frac{1}{M}[\beta_B(m_T - E_S) + p_S \cos\theta], \tag{3}
$$

17

Table 4: Estimated energy resolution from individual terms in MeV.

	Δp_B	Δp_S	$\Delta \theta$		$\Delta E_{\text{strag.}}$	ΔM
H$(K^-, K^+)\Xi^-$	0.39	1.56	0.30	1.64	<2.0	<2.6
^{12}C$(K^-, K^+)^{12}_\Xi$Be	0.56	2.26	0.04	2.33	<2.0	<3.1

$$\frac{\partial M}{\partial p_S} = -\frac{1}{M}[\beta_S(m_T + E_B) - p_B \cos \theta], \tag{4}$$

$$\frac{\partial M}{\partial \theta} = -\frac{1}{M} p_B p_S \sin \theta, \tag{5}$$

where β_B and β_S are velocities of the beam and scattered particles, respectively. Δp_B, Δp_S and $\Delta \theta$ are resolution of the measurements of momenta of the beam and scattered particles and scattering angle, respectively.

Momentum resolution of the beam analyzer at 1.8 GeV/c is $1.4 \times 10^{-4} \times 2.355 \times 1800 = 0.6$ MeV/c(FWHM), while that of the K^+ spectrometer is assumed to be 2.5 MeV/c(FWHM). In Table 4, the expected energy resolution for each reaction at scattering angle of 5° are listed assuming spectrometer resolution above and angle resolution of 2 mrad. The contribution of the individual terms are also listed. Energy resolution is mainly determined by the K^+ spectrometer as well as the energy loss straggling in the target. In order to keep the resolution within the acceptable level, c.f. 3 MeV, the energy loss straggling should be less than 2 MeV. Thus, maximum thickness of a target is $5 - 6$ g/cm^2.

3.4   Backgrounds and Trigger Rate

There is no physical background in the region of our interest except for the production of double-Λ hypernuclei and a continuum component producing a single-Λ fragment with one Λ escaping. However, these states are of our another interest and can be easily separated from the Ξ-hypernuclear states with a good energy resolution. The quasi-free Ξ^- production is a main contribution in the (K^-, K^+) reaction. Thus misidentification of the beam and/or scattered particles as well as a wrong reconstruction of the momentum are possible background sources. However they seems to be within our acceptable level.

Because of the double-charge-exchange reaction, the beam particles and negatively charged particles are swept out by the first dipole. Therefore, negatively charged particles such as K^- from an elastic scattering, π^- and μ^- from K-decay, cannot reach the trigger counters. The rate of K^+ is determined by the quasi-free Ξ production. The cross section on carbon target was measured to be 99$\pm$4 μb/sr at 1.65 GeV/c[30]. On the other hand, momentum of the K^+ associated with Ξ^{*-} production is out of the spectrometer acceptance. Assuming the beam intensity of 2 MHz and neglecting the

18

decay factor, true K^+ trigger rate is estimated as,

$$
\begin{aligned}
R(K^+) &= R_{beam} \times N_{target} \times \frac{d\sigma}{d\Omega} \times \Delta\Omega \qquad &(6)\\
&= 2 \times 10^6 [\text{Hz}] \times \{5.4 \times 6.02 \times 10^{-7}/12\}[/\mu\text{b}] \times 100[\mu\text{b/sr}] \times 0.030[\text{sr}]\\
&= 1.63 [\text{Hz}]. &(7)
\end{aligned}
$$

Three order of magnitude higher rates are expected for π^+ and protons than that for K^+. The pions, however, can be easily suppressed by the existing AC in the trigger level. Suppression more than 99% has been achived in the SKS experiments at KEK-PS, although the momentum region is different; $\sim$0.7 GeV/c for KEK-PS, while $\sim$1.3 GeV/c for J-PARC. Thus protons are main trigger backgrounds and have to be suppressed by at least 10% level. The existing LC ($n = 1.49$) is not efficient for p/K^+ discrimination in this momentum region, although they can be somewhat separated by the light outputs. Therefore, we are going to prepare a water ($n = 1.33$) Cerenkov counter. Another choice is to use an aerogel counter with the index of $\sim$1.2, which has been recently available. A counter of small-size can be installed downstream of the target, though it may affects the energy resolution.

Anyway, trigger rate of several hundreds Hz can be handled by the existing front-end modules such as TKO and VME as well as a new DAQ system.

4   Yield Estimation

The production cross sections of the Ξ-hypernuclei in the (K^-, K^+) reaction have been calculated by several theorists within the framework of distorted-wave impulse approximation (DWIA)[31, 32]. In the calculation using the Kapur-Peiers method assuming Woods-Saxon type potential for Ξ^- in the nuclei,

$$
\begin{aligned}
V(r) &= \frac{V_0^\Xi}{1 + \exp((r - R)/a)}, &(8)\\
R &= r_0(A - 1)^{1/3} &(9)
\end{aligned}
$$

with $r_0 = 1.1$ fm and $a = 0.65$ fm, the forward angle laboratory cross section for $^{12}\text{C}(K^-, K^+)^{12}_\Xi\text{Be}(s\text{-state})$ at $p = 1.6$ GeV/c is estimated to be from 215 to 81 nb/sr for the potential depth of $V_0^\Xi = -24$ to -12 MeV[31]. Another calculation using Green function method and the complex Woods-Saxon potential[32] gives similar results; 250 nb/sr for $V_0^\Xi = -24$ MeV. Table 5 summarizes the calculation results.

On the other hand, experimental studies reported cross sections, although they could not observe the bound states clearly due to the insufficient experimental resolution and statistics[9, 10]. The BNL AGS-E885 reported that the cross section for $^{12}\text{C}(K^-, K^+)^{12}_\Xi\text{Be}$ reaction at p=1.8 GeV/c is 89±14 and 42±5 nb/sr for the angular average from 0° to 8° and from 0° to 14°, respectively[10], while KEK-PS-E224 reported 0.21±0.07 μb/sr for the region of $E_\Xi \leq 7$ MeV, which is angular averaged from

19

Table 5: The calculated cross sections at $0°$ for $^{12}\mathrm{C}(K^-, K^+)^{12}_{\Xi}\mathrm{Be}$ reaction at $p = 1.6$ GeV/c for various potential depths from [31].

states		V_0^Ξ [MeV]			
		-24	-20	-16	-12
s-state					[nb/sr]
$0p_{3/2} \to 0s_{1/2}$	1^-	215	168	123	81
p-states					[nb/sr]
$0p_{3/2} \to 0p_{3/2}$	0^+	29	20	—	—
	2^+	164	103	—	—
$0p_{3/2} \to 0p_{1/2}$	2^+	152	93	—	—
sum		345	216	—	—

$0°$ to $12°$ at p=1.65 GeV/c[9][1]. Here we take 60 nb/sr for carbon target, taking into our angular acceptance of from $0°$ to $10°$.

For the number of K^-, we can expect 3.7×10^{10}/day for 1.4×10^6 [/spill] when we choose flat-top length of 0.8 second, which corresponds to the singles-rate of 2.0 MHz at the target as shown in Fig.11.

Thus the yield of $^{12}_{\Xi}\mathrm{Be}$ is estimated as follows,

$$
\begin{aligned}
Y(^{12}\mathrm{C}) &= N_{beam} \times N_{target} \times \frac{d\sigma}{d\Omega} \times \Delta\Omega \times f_{decay} \times f_{analysis} \quad (10) \\
&= 3.7 \times 10^{10} [/\mathrm{day}] \times \{5.4 \times 6.02 \times 10^{-7}/12\}[/\mu\mathrm{b}] \\
&\quad \times 0.06[\mu\mathrm{b/sr}] \times 0.030[\mathrm{sr}] \times 0.5 \times 0.7 \\
&= 6.3[/\mathrm{day}] \\
&\sim 45[/\mathrm{week}] \\
&\sim 190[/\mathrm{month}]. \quad (11)
\end{aligned}
$$

Therefore, we need $\sim$1 month data-taking for $^{12}\mathrm{C}(K^-, K^+)^{12}_{\Xi}\mathrm{Be}$ reaction. For heavier targets, production cross sections are not reliably calculated since Ξ^- potential depth, especially the A-dependence, is not known at all. Even if the cross section is as large as that for the carbon target, the yield is proportional to $1/A$ from the target thickness due to the energy resolution.

On the other hand, the cross section for $\mathrm{H}(K^-, K^+)\Xi^-$ which is used for tuning and calibration of the beam and K^+ spectrometers, was measured to be 35 ± 4 μb/sr at 1.65 GeV/c[30]. The yield for the elementary Ξ^- production using CH_2 target with 5 g/cm^2 is estimated as,

$$
Y(\mathrm{elem}) = 3.7 \times 10^{10}[/\mathrm{day}] \times \{5 \times 6.02 \times 10^{-7} \times 2/(2+12)\}[/\mu\mathrm{b}]
$$

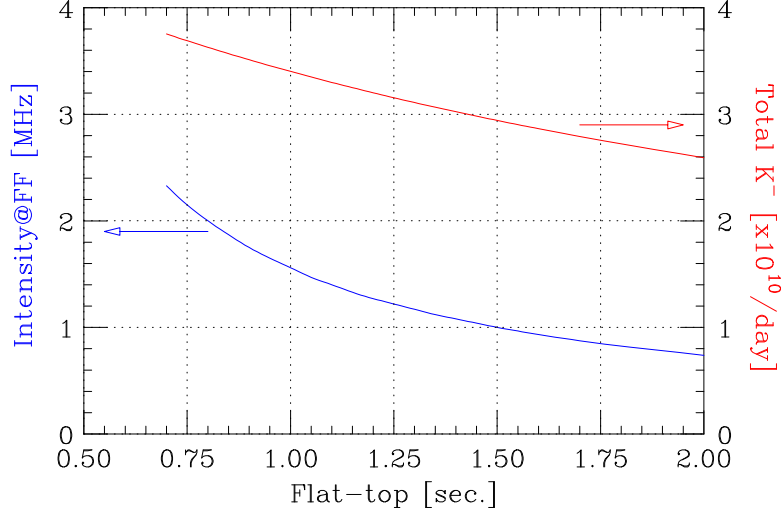[1]In ref.[10], cross section for E224 is cited to be 60 ± 45 nb/sr for the bound region.

Figure 11: The instantaneous beam intensity and total number of K^- per day against flat-top length of the accelerator operation.

$$\times 35[\mu b/sr] \times 0.030[sr] \times 0.5 \times 0.7$$
$$= 5.8 \times 10^3 [/day]. \tag{12}$$

This number is large enough for performance study of spectrometers, tuning, and calibration.

5 Requested Beam Time

Here we summarize the requested beam time.

- **Stage.0**
  K1.8 beam line study and tuning for K^- beams
  3 – 4 weeks

- **Stage.1**
  Detector tuning, trigger tuning etc. Spectrometer performance check such as optics, resolution, and acceptance using CH_2 target.
  2 weeks

- **Stage.2**
  Measurement of $^{12}C(K^-, K^+)_\Xi^{12}Be$ reaction.
  4 weeks

- **Stage.3** (future extension)
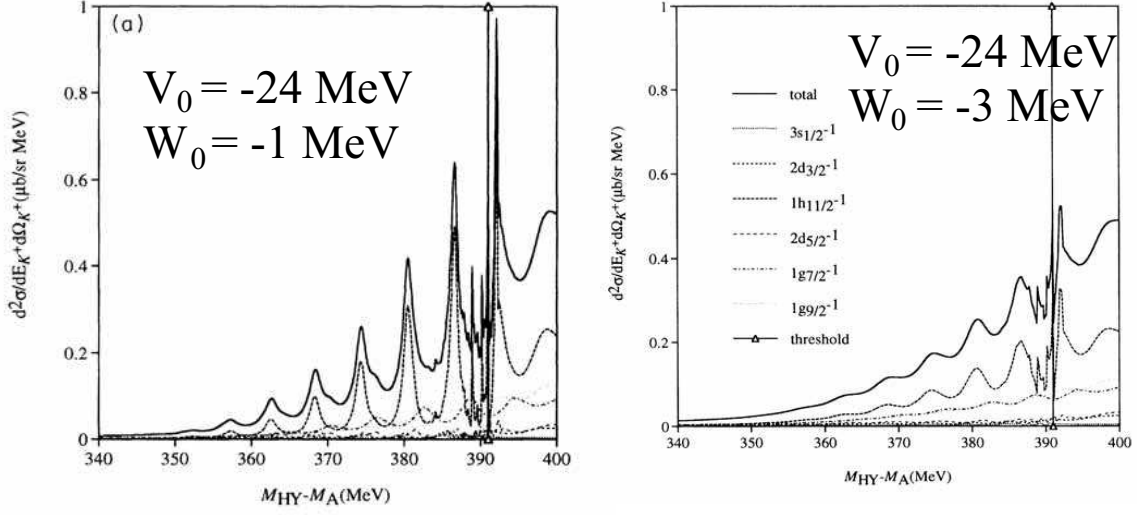 Measurement on a heavy target, for example, ^{89}Y.
  3 months

21

Figure 12: The calculated spectra for ^{208}Pb(K^-, K^+) reaction taken from ref[32]. Real part of the Woods-Saxon potential is taken to -24 MeV, while imaginary part is taken to -1 MeV (left) or -3 MeV (right).

Studies at Stage.1 can be performed with lower beam intensity, c.f. 10% of the full beam intensity, because the production yield for the elementary process is large enough for the spectrometer optics study, etc. The operation and performance studies for the beam line counters under high-rate circumstance can be done shortly by using π^- beams instead of K^-.

At Stage.2, however, full intensity or at least half of the full intensity beam at Phase 1 is needed. Here, the full intensity means so-called 30 GeV-9 μA primary beam which corresponds to $1.4 \times 10^6 K^-$ [/spill].

At Stage.3, although we have no intention to request the beam time at this moment, we will require higher beam power, by means of 15 μA operation or beam energy upgrade, etc.

6   Future Extension

Although the measurement on ^{12}C target proposed here is a significant and essential step to investigate Ξ-hypernuclei, it is necessary to extend the measurements for a variety of targets to fully explore plentiful physics in the $S = -2$ and multi-strangeness systems.

Two directions are considered to extend our studies on Ξ-hypernuclei and ΞN interaction.

One is to go on heavier targets to measure the A-dependence of the single-particle potential of Ξ by using a few targets in a wide mass number range. As described

in "Introduction", the A-dependence of Ξ-binding energies has a key information for discriminating the underlying ΞN interaction models. The measurement with heavy targets is also essential to obtain the Ξ-potential in nuclear matter at normal density, which is necessary in the study of high-density hadronic matters such as a core of neutron star.

Furthermore, for heavy nuclei, the Coulomb force becomes more attractive to bind Ξ^- more deeply (so-called Coulomb-assisted states). It is also argued that very narrow peaks with a large orbital angular momentum can be observed in the heavy Ξ-hypernuclei as shown in Fig.12. In such states, a Ξ^- stays at the surface region of low nucleon density due to strong centrifugal barrier. Therefore, the $\Xi N \to \Lambda\Lambda$ conversion is suppressed, and the conversion width is reduced. Since large production cross sections can be expected for such peculiar states, it may be possible to observe such states within a reasonable beam time, if we could increase the primary beam intensity with 15-bunch operation. For example, in the ^{89}Y case, the number of events is expected as

$$
\begin{aligned}
N(^{89}\text{Y}) &= N(^{12}\text{C}) \times \frac{12}{89}(\text{thickness}) \times \frac{15}{9}(\text{intensity}) \times 2.4(\text{time}) \times f \\
&= 0.54 f N(^{12}\text{C}) \geq 100 (f \geq 1),
\end{aligned}
\tag{13}
$$

where f is the cross section ratio between ^{12}C and ^{89}Y targets.

The other direction is a search for p-n-Ξ^- (n-n-Ξ^0) state via the $^3\text{He}(K^-, K^+)$ reaction. The existence of this bound state strongly depends on the spin-isospin structure of the ΞN interaction. At present, there is no reliable theoretical prediction whether this three-body system is bound or not. If it is bound, however, this system might play an important role in the study of ΞN interaction like a deuteron in the NN interaction.

7   Schedule and Cost Estimate

We are going to recycle or reuse the detectors in the existing SKS spectrometer system as many as possible when they fit for the (K^-, K^+) spectroscopy, including the readout and front-end electronics. However, several components should be newly constructed dedicated for the J-PARC experiment, such as beam line detectors including their readout and an additional dipole magnet, by using the budget (Kakenhi) of the Grant-In-Aid for Priority Areas, "Multi-quark systems with strangeness" (2005 – 2009). These items are listed in Table 6.

Figure 13 shows the time schedule of the preparation for the proposed experiment. The beam line detectors and their readout will be fabricated first with the highest priority by the Kakenhi budget.

In addition to those instruments prepare by the experimental group, K1.8 beam line including the beam analyzer system, and the SKS spectrometer without the additional dipole magnet should be prepared by the J-PARC construction team as planned. Of course, the experimental group is willing to work together from the installation. As for the superconducting magnet of the SKS, the present large refrigerator system will
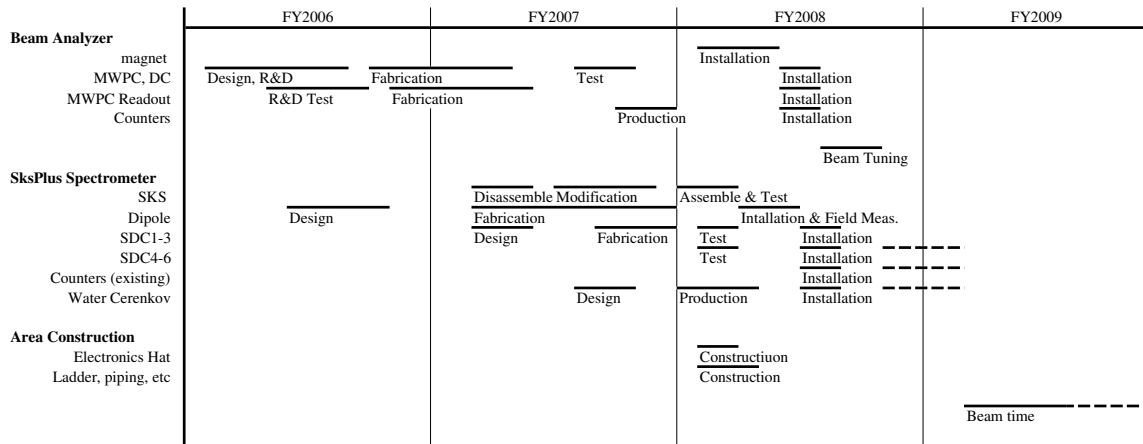
Figure 13: Schedule of the preparation for the proposed experiment

be replaced by several small-sized GM-JT refrigerators with some modifications of the coil and helium vessels. It will allow us for easy operation and maintenance with the estimated cost of ∼200M JYen in total.

Table 6: A list of items needed for this experiment

Item		Cost [kJY]	
Beam Analyzer			
1mm MWPC ×2	New	4,000	Kakenhi
3mm DC ×2	New	3,000	Kakenhi
Readout Amp.& Discri.	New	9,000	Kakenhi
MWPC Encoder	New	20,000	Kakenhi
DC MultiHit TDC	Existing	0	
Beam Hodoscope	New	3,000	Kakenhi
Beam Aerogel Counters	New	1,000	Kakenhi
Support Frame etc.	New	2,000	
SksPlus Spectrometer			
Dipole Magnet	N/R	30,000	Kakenhi
Power Supply	N/R		
DC (SDC1–3)	New	25,000	Kakenhi
DC (SDC4–6)	Existing		
TOF	Existing	1,000	Kakenhi
AC ×2	Existing	2,000	Kakenhi
LC	Existing	1,000	Kakenhi
Water Cerenkov Counters	New	10,000	Kakenhi
Readout Amp.& Discri.	New	6,000	Kakenhi
DC M.H.Tdc and DrT-II	Existing	0	
Support Frame etc.	New	5,000	
Area Construction etc.			
Electronics Hat	Reuse	5,000	
SKS Ref. Control Hat		8,000	
AVR etc.	Recycle	4,000	
Cable Ladder	New	5,000	
Gas piping, alarm system	New	7,000	
Gas mixer system	Existing		
Cables	N/R	10,000	Kakenhi
Electronics etc.			
PMT P.S.'s	Existing		Electronics Pool
Racks, Bins, Crates etc	Existing		Electronics Pool
NIM, CAMAC, TKO modules	Existing		Electronics Pool
Discriminators	New	3,000	Kakenhi
Trigger Logic (FPGA)	New	2,000	Kakenhi
DAQ System	New	2,000	Kakenhi
Analysis Computer System	New	6,000	Kakenhi
Data Storage	New	6,000	Kakenhi
VME Crates and P.S.'s	New	2,000	Kakenhi

A ΞN Interaction Models and Ξ-Potentials

Since little is known for $S = -2$ baryon-baryon systems, there is no established interaction model in $S = -2$ channels. SU(3)-invariant interaction models give useful predictions for unknown $S = -2$ sectors. The derived one-body Ξ potentials U_Ξ, however, are remarkably different among interaction models. Here, we pick up the following three interaction models, which give attractive (negative) values of U_Ξ:

- Nijmegen Hard-Core model D (NHC-D)[18]

- Ehime model[19]

- Extended Soft-Core model 04d* (ESC04d*)[20]

NHC-D and Ehime are One-Boson-Exchange (OBE) potentials. In these models, there appear the following important features:

1. When the scalar-meson nonet (octet+singlet) are taken into account straightforwardly, the derived ΞN interactions are not attractive enough to give attractive values of U_Ξ. In the cases of NHC-D and Ehime, the attractive U_Ξ's are owing to the following peculiar modeling: In the NHC-D case, only the unitary-singlet σ meson is included with neglect of octet scalar mesons, which gives universal attractions in all baryon-baryon (BB) channels. In the Ehime case, the additional σ meson is included together with the nonet mesons.

2. In ΞN channels, strangeness -2 cannot be carried by a single boson, which leads to no space-exchange term. Namely, the OBE parts of odd-state interactions are the same as those of the even-state ones. Thus, the attractive values of U_Ξ are of large contributions from odd-state attractions, which brings about a strong mass number (A) dependence of U_Ξ; even if the U_Ξ's are shallow in light systems, the deep values are expected in heavy systems.

3. In the case of NHC-D (Ehime), the hard-core radii (the coupling constant $g_{\Xi\Xi\sigma}$) can be adjusted so as to reproduce the appropriate value of U_Ξ. In the present calculations, they are adjusted so that the derived Ξ-^{11}B potentials are similar to the Woods-Saxon potential with the depth of -14 MeV.

On the other hand, the features of the recent model ESC04d* are very different from those of the above OBE models.

1. All exchange mesons and their coupling constants are of physical meaning, namely no effective boson is included. The interaction parameters in $S = -2$ channels are derived uniquely from those in $S = 0$ and -1 channels.

2. Even in ΞN channels, strangeness -2 can be carried by meson pairs, which lead to space-exchange terms. Then, the odd-state interactions in ESC04d* are far

less attractive than those in the above OBE models. An attractive value of U_Ξ is owing to the strong attraction in the $^3S_1(T=0)$ state. This attraction produces peculiar Ξ bound states in s- and light p-shell systems, differently from the cases of NHC-D and Ehime.

3. The ΞN-$\Lambda\Lambda$ coupling interaction in ESC04d* is far stronger than those in NHC-D and Ehime. This feature is due to the meson-pair exchange terms in ESC04d*.

The deep values of Ξ potential in nuclear matter at normal density, U_Ξ, for NHC-D and Ehime in Table 1 are owing to the strong odd-state attractions, whose contributions are not so large in light systems. In the case of ESC04d*, the large attractive contribution in the $^3S_1(T=0)$ state turns out to be decisive role for the negative value of U_Ξ. Another important difference between ESC04d* and NHC-D/Ehime is that the conversion width for the former is far larger than those for the latters.

The energies and widths, which is listed in Table 2, for Ξ^- bound states are calculated by the spin- and isospin-averaged Ξ-nucleus potentials derived by folding the ΞN G-matrix interactions into Skyrme-Hartree-Fock nuclear-core wave functions[17]. Calculations are performed with and without Coulomb interactions. Here, it should be noted that the Ξ^- s-state energies in $^{12}_{\Xi^-}$Be are more or less similar to each other. The differences turn out to become substantial with increase of mass numbers A. Therefore, the experimental information on the A-dependence of Ξ-binding energies is indispensable for discriminating the underlying ΞN interaction models. It is also important that calculated conversion widths for ESC04d* and NHC-D/Ehime are very different from each other.

In order to obtain more realistic energies for Ξ bound states, one should add interaction energies between Ξ-particle and nucleon-hole (N^{-1}) on the above Ξ binding energies. For instance, the estimated values for $\langle (s_{1/2})_\Xi (p_{3/2})_p^{-1} | V_{\Xi N} | (s_{1/2})_\Xi (p_{3/2})_p^{-1} \rangle_{TJ}$ in $^{12}_{\Xi^-}$B are as follows (in MeV):

TJ	NHC-D	Ehime	ESC04d*
01	+0.7	+0.9	−1.2
02	+0.5	+0.4	−0.5
11	+0.3	+0.6	+2.2
12	+1.0	+0.6	+0.2

These values indicate that the Lane potentials for NHC-D and Ehime are weak, and the one for ESC04d* is strongly repulsive. It should be noted that only $T=1$ $\Xi^- p^{-1}$ states are produced by (K^-, K^+) reaction. In addition, due to a large momentum transfer in this reaction, the $J=2$ state is expected to be more strongly excited than the $J=1$ state.
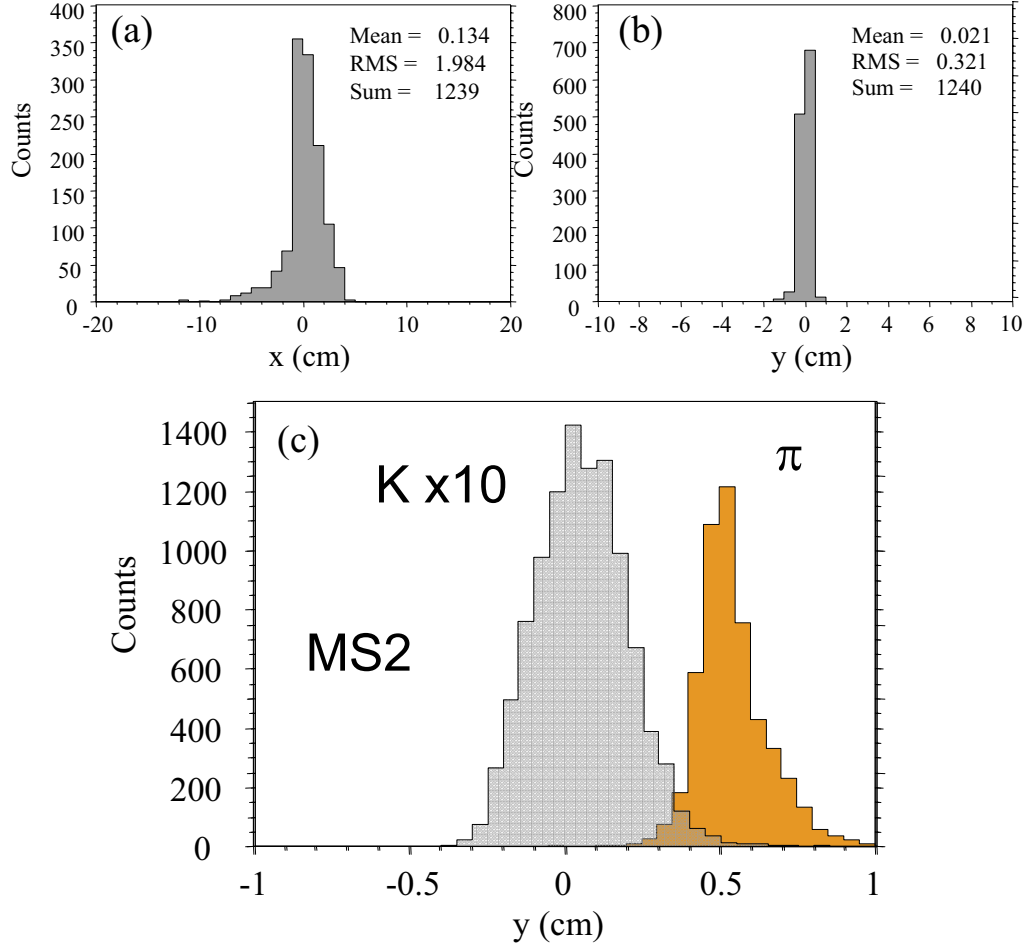
Figure 14: The horizontal (a) and vertical (b) images at the final focus (F.F.) of the K1.8 beam line. Beam image for kaons and pions at MS2 is drawn in figure (c).

B   K1.8 Beam Line

Here, we briefly summarize the details of the design status of the K1.8 beam line to be constructed.

In the current design, one of the most serious problems which should be considered is the high radiation levels surrounding the production target. There, about 30% of the primary proton power will be lost and distributed around the target. Thus, radiation hardness of the materials to be used in the equipment near the production target is required. Also, we should consider the cooling to remove the heat load in these materials. Therefore, new magnets with mineral-insulation coils will be constructed in the front end of the beam line, while most of the downstream magnets are existing ordinary magnets. The first electro-static separator in the upstream has been also

Table 7: Characteristics of the magnets and other elements of the K1.8 beam line

| Name	Gap/Bore [mm]	Width [mm]	Length [mm]	Field [kG]	Tot. Len. [m]		
T1					0.000		
D1	80	200	800	13.10	1.200	New	in vacuum
Q1	160		600	7.60	2.400	New	in vacuum
Q2	200		800	−7.41	3.600	Recycle	
D2	120	350	900	17.47	4.800	New	15° bend
IF					5.900		
Q3	200		500	7.90	7.000	Recycle	
O1	250		150	1.00	7.675	New	
Q4	200		500	−8.80	8.000	Recycle	
S1	250		200	0.57	8.800	New	
CM1	250	200	200	3.76	9.300	New	
ES1				6.20	9.600	New	
CM2	250	200	200	3.76	16.100	New	
S2	250		200	−1.44	16.600	Recycle	
Q5	250		500	8.20	17.100	Recycle	
Q6	300		500	9.17	18.200	Recycle	
MS1					19.300		
D3	170	1000	1500	14.12	20.200	Recycle	20° bend
Q7	200		400	8.20	22.284	Recycle	
O2	300		150	1.75	22.8347	New	
S3	300		200	−1.59	23.1347	New	
CM3	300	300	200	3.76	23.6347	Recycle	
ES2				6.50	24.0347	Recycle	PS-K6
CM4	300	300	200	3.76	30.4347	Recycle	
S4	300		200	0.25	30.9347	New	
Q8	250		600	−8.90	31.4347	Recycle	
O3	300		150	1.25	32.1847	New	
Q9	250		900	10.35	32.4847	Recycle	
MS2					33.8348		
Q10	200		900	9.79	35.5848	Recycle	
Q11	200		600	9.79	36.7848	Recycle	
D4	200	660	4468	15.01	37.8848	Recycle	64° bend
Q12	200		600	8.50	42.8528	Recycle	
Q13	200		600	-6.70	43.7528	Recycle	
FF					45.8530		

29
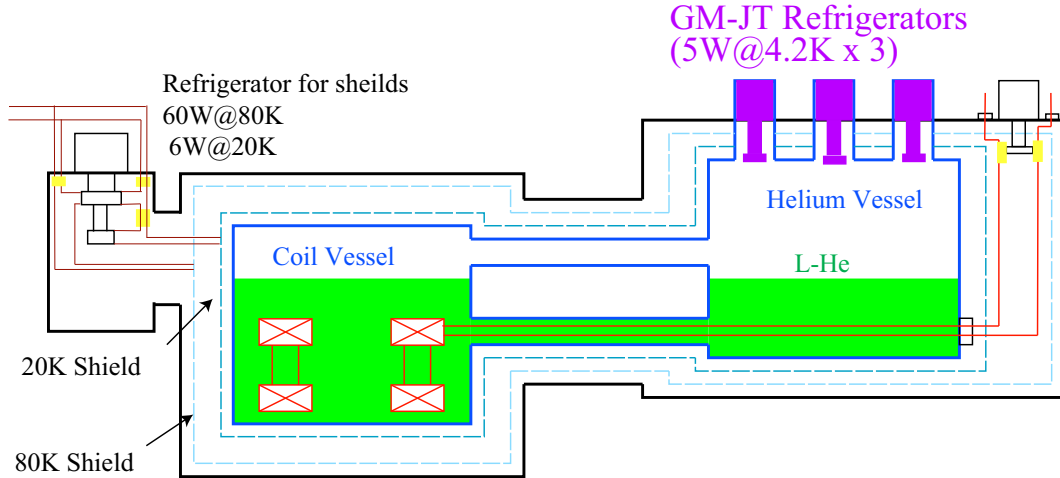
Figure 15: A conceptual design of the new cryogenic system for the SKS magnet. The liquid state of the helium coolant is always kept by 3 GM-JT refrigerators.

newly constructed with several improvements against high radiation level, and tested showing a good performance. In Table 7, we show which equipment is going to be newly constructed for the K1.8.

The tuning of the beam optics to obtain a good K^-/π^- ratio has been carried out by H. Noumi et al., already. Higher order corrections up to the 3rd order was taken into account with four secta-pole magnets and three octa-pole magnets. Figures 14 shows an example of the tuning simulation of the beam profile at the final focus point and of the K^-/π^- separation at the second mass slit.

C   New Cryogenic System for SKS

The SKS superconducting magnet was designed to minimize the heat load at 4 K. Although we have been using a large cryogenic system to cool down the magnet, it was suggested that several small refrigerators could be used for the SKS magnet because of the recent refrigeration power improvements in this type of small refrigerator system. It will reduce the costs to transfer the SKS spectrometer system with the cryogenic system from Tsukuba to Tokai. Also the operation of the cryogenic system will be simplified and become easier. Since the system is not controlled under the regulation for high-pressure gas system, the maintenance is also much easier.

In Fig.15, we show a conceptual design of the new cryogenic system for the SKS magnet.

References

[1] K. Imai, *et al.*, Letter of Intent for Nuclear and Particle Physics Experiments at the J-PARC, KEK, L06 (2003), http://www-ps.kek.jp/jhf-np/LOIlist/pdf/L06.pdf.

[2] C. B. Dover and A. Gal, Ann. of Phys. **146**, 309 (1983).

[3] M. Danysz, *et al.*, Nucl. Phys. **49**, 121 (1963).

[4] R. H. Dalitz, *et al.*, Proc. Roy. Soc. Lond. **A426**, 1 (1989).

[5] D. J. Prowse, Phys. Rev. Lett. **17**, 782 (1966).

[6] S. Aoki, *et al.*, Prog. Theor. Phys. **85**, 1287 (1991).

[7] H. Takahashi, *et al.*, Phys. Rev. Lett. **87**, 212502 (2001).

[8] J. K. Ahn, *et al.*, Phys. Rev. Lett. **87**, 132504 (2001).

[9] T. Fukuda, *et al.*, Phys. Rev. C **58**, 1306 (1998).

[10] P. Khaustov, *et al.*, Phys. Rev. C **61**, 054603 (2000).

[11] G. Burgen, *et al.*, Nucl. Phys. **B8**, 447 (1968).

[12] P. M. Dauber, *et al.*, Phys. Rev. **179**, 1262 (1969).

[13] D. E. Lanskoy, private communication.

[14] P. H. Pile, *et al.*, Phys. Rev. Lett. **66**, 2585 (1991).

[15] T. Hasegawa, *et al.*, Phys. Rev. Lett. **74**, 224 (1995).

[16] H. Hotchi, *et al.*, Phys. Rev. C **64**, 044302 (2001).

[17] Y. Yamamoto, private communication.

[18] M. M. Nagels, Th. A. Rijken and J. J. de Swart, Phys. Rev. D **15**, 2547 (1977).

[19] M. Yamaguchi, K. Tominaga, Y. Yamamoto and T. Ueda, Prog. Thoer. Phys. **105**, 627 (2001).

[20] Th. A. Rijken and Y. Yamamoto, Phys. Rev. C, to be published; arXiv:nucl-th/0603042.

[21] T. Nagae, *et al.*, Phys. Rev. Lett. **80**, 1605 (1998).

[22] T. Suzuki, *et al.*, Phys. Lett. B **597**, 263 (2004).

[23] M. Agnello, *et al.*, Phys. Rev. Lett. **94**, 212303 (2005).

[24] T. Kishimoto, *et al.*, Nucl. Phys. A **754**, 383c (2005).

[25] E. Hiyama, Nucl. Phys. **A670**, 273c (2000).

[26] I. N. Filikhim and A. Gal, Phys. Rev. Lett. **89**, 172502 (2002).

[27] H. Nemura, Y. Akaishi and Khin Swe Myint, Phys. Rev. C **67**, 051001(R) (2003).

[28] E. Hiyama, *et al.*, Nucl. Phys. **A737**, 138 (2004).

[29] A. J. Baltz, C. B. Dover, D. J. Millener, Phys. Lett. B123, 9 (1983).

[30] T. Iijima, *et al.*, Nucl. Phys. **A546**, 588 (1992).

[31] K. Ikeda, T. Fukuda, T. Motoba, M. Takahashi and Y. Yamamoto, Prog. Theor. Phys. 91, 747 (1994); Y. Yamamoto, T. Motoba, T. Fukuda, M. Takahashi and K. Ikeda, Prog. Theor. Phys. Suppl. 117, 281 (1994).

[32] S. Tadokoro, H. Kobayashi, and Y. Akaishi, Phys. Rev. C **51**, 2656 (1995).